Journal of
Materials Chemistry A

Materials for energy and sustainability

Accepted Manuscript

This article can be cited before page numbers have been issued, to do this please use: H. Lin, W. Ye, Y. liu, M. liu, C. Song, H. Zhang, R. Lu and S. Zhang, *J. Mater. Chem. A*, 2019, DOI: 10.1039/C9TA10808D.

ROYAL SOCIETY OF CHEMISTRY

rsc.li/materials-a

View Article Online
DOI: 10.1039/C9TA10808D

Controlling Solubility: A Chemistry Approach toward Preparing Nitrogen-Doped Hollow Carbon Nanospheres

Hua Lin, Wanyue Ye, Yingcen Liu, Minghui Liu, Caicheng Song, Hao Zhang, Rongwen Lu* and Shufen Zhang

State Key Laboratory of Fine Chemicals, Dalian University of Technology, Dalian 116024, China

Corresponding Author: Rongwen Lu, E-mail: lurw@dlut.edu.cn

Abstract

Nitrogen-doped hollow carbon nanospheres have inspired considerable attention in various fields such as catalysis, biomedicine, adsorption and energy storage/conversion. The most widely used methods are template-based routes. However, the operating procedures are tedious and the mechanism of formation process is still unclear. Here, we have designed a new protocol to synthesize nitrogen-doped hollow carbon nanospheres by preparing and post-treating nanospheres with area-specific distribution, which is guided by the solubility control through the whole synthesis process. The hollow inner structure was formed based on the reversibility of chemical reactions without any template assistance. The forming mechanisms of novel solid polymer spheres and the hollow structure have been investigated. The size, morphology and shell thickness of spheres could be tuned by changing the amount of reactants, the ratio of acetone/water and subsequent treatment process. Furthermore, the nitrogen-doped hollow carbon nanospheres exhibited both high stability and capacity as Li-S battery cathode with a capacity of 528 m Ah g^{-1} after 300 cycles at 0.5C.

1. Introduction

Hollow carbon spheres (HCSs) are continuously under the public attention due to their novel

View Article Online
DOI: 10.1039/C9TA10808D

structural and multi-functional characters, receiving attention in various areas of academic and industrial research such as energy conversion/storage (lithium-sulfur battery[1-3], super-capacitance[4, 5], fuel cell[6-8], etc[9].), catalysis[10, 11], water and air treatment[12, 13], and biomedicine[14]. The synthesis design and structure optimization give HCSs several novel features such as controllable pore structure, surface properties, and cavity, which leaves huge space for further control of their functionalities and architectures to achieve optimization of application property.

For the synthesis of HCSs, template-assisted routes are commonly used to make hollow structure, involving hard template and soft template method. Generally, hard template method using various monodispersed materials including silica,[15-18] polymer,[19, 20] and other nanoporous solid[21, 22] can produce uniform and dense cavity, but the remove of template usually need high temperature (over 600 °C)[19, 20, 22], dissolution or acid/alkaline etching. Some researchers employed emulsions,[23] micelles[24] or bubbles[25] as soft template for the production of HCSs, nevertheless, finding suitable templates is challengeable by the limited choice of surfactant and the insufficient shape control of hollow structure[26]. Other methods such as ostwald ripening,[27] and pyrolysis[28] are generally conducted under more than 150 °C[29, 30] and harsh reaction conditions. Thus, it is necessary for us to develop a facile synthetic method which can rapidly create uniform hollow architectures under mild condition, as well as further insights into the formation mechanism. Wan et al. have done pioneering work for synthesizing multishelled hollow carbon spheres using 3-aminophenol/formaldehyde resin at room temperature. Resin nanospheres with inner different degree of polymerization were formed and their growth kinetics could be tuned by controlling the reaction condition.[26] Such novel method has rarely been reported for the fabrication of hollow structure, even the mechanism of cavity formation by the solvent effect.

View Article Online
DOI: 10.1039/C9TA10808D

Thus, developing new polymer precursors to prepare carbon spheres with a changeable internal structure has a great significance for the extend investigation of nitrogen-doped hollow carbon nanospheres.

Herein, by projecting the heterogeneous components inside the single nanoparticles, we proposed a new protocol that polymeric nanospheres themselves act as a platform to create inner hollow structure via altering the solubility of reactant and product. Specifically, polymer spheres with uniform shape but different inner and outer chemical constitution have been successfully synthesized based on Schiff base chemistry. The formation mechanism of this novel solid polymer spheres has been explored for understanding the whole structure of the spheres. It is suggested that the hollow structure could be formed according to the reversibility of chemical reactions at room temperature (25 °C), which provided a new strategy to build different hollow architectures. The as-prepared polymer hollow spheres contain large quantities of nitrogen (27.0% in HPSs), which can be attributed to the abundant nitrogen source in melamine. After calcination and further activation, the HCSs show good electrochemical performance in Li–S batteries benefiting from hollow cavities, rich porous structure and high nitrogen content (12.5% in HCSs).

2. Experimental section

2.1 Chemicals

3,5-Diaminobenzoic acid (≥98.0%) was purchased from Energy Chemical (Shanghai, China). Melamine and formaldehyde (37%~40%) were purchased from Sinopharm Chemical Reagent Co., Ltd. (Shanghai, China). Ammonia solution ($NH_3 \cdot H_2O$, 25%~28%) and m-phenylenediamine were obtained from Damao Chemical Reagent Factory (Tianjin, China). All chemicals were AR-grade and used without further purification. Deionized water was used in all experiments.

View Article Online
DOI: 10.1039/C9TA10808D

2.2 Synthesis of Solid Polymer Spheres (SPSs) and Hollow Polymer Spheres (HPSs)

First, *m*-phenylenediamine (0.054 g), melamine (0.063 g) and 3,5-diaminobenzoic acid (0.047 g) were added to the mixture solvent of 45 mL acetone and 5 mL deionized water. The mixture was dispersed by ultrasound until a light brown suspension appeared. Then, under magnetic stirring, 0.2 mL ammonia solution ($NH_3 \cdot H_2O$, 25%~28%) and 2 mL formaldehyde solution (37%~40%) were added into the system, respectively. After 6 h of reaction, a yellow suspension was obtained and the products were collected by centrifugation at 8000 rpm for 6 min. The obtained solid polymer spheres (SPSs) were transferred to a 50 mL flask, followed by pouring 30 mL formaldehyde solution (37%~40%). After that, the mixture was stirred for one hour at room temperature (25 °C). Subsequently, the resulting precipitates were centrifuged at 8000 rpm for 6 min and washed three times with methyl alcohol. In the end, the yellow product (HPSs) was obtained and dried at 60 °C overnight under vacuum condition. The yields of SPSs and HPSs were 79.8% and 58.0%, respectively.

2.3 Synthesis of Hollow Carbon Spheres (HCSs)

The HPSs sample undergone a temperature-programmed calcination with a specific program. The HPSs were heated to 200 °C and continued for 60 min, then calcined to 300 °C with a heating rate of 1 °C/min and held for 1 h; subsequently the sample were further heated to 700 °C with a heating rate of 5 °C/min and kept for 1 h. The whole process was performed under an argon atmosphere. For activation, the obtained HCSs (300 mg) were mixed with 1.5 g K_2CO_3 dissolving in 30 mL water and transferred into the crucible, forming a homogeneous slurry under magnetic stirring. The sample was dried at 105 °C in oven, afterward the mixture was calcined at 800 °C for

View Article Online
DOI: 10.1039/C9TA10808D

2 h under nitrogen atmosphere to yield activated carbon spheres. At last, the product was washed with HCl (1 M) solution and deionized water to remove the residue of K_2CO_3. The mass ratio of K_2CO_3 and carbon spheres was 5:1. The finial sample was named HCSs-5.

2.4 Preparation of (HCSs-5-S) composites

The mixture of HCSs-5 and sulfur powder with mass ratios of 1:2 were heated at 155 °C for 6 h in a sealed glass vessel under Ar protection. Subsequently, the temperature was increased to 400 °C with a heating rate of 2 °C/min and kept for 1 h to ensure the sulfur penetration into the spheres, which can also remove the residual sulfur from outer surface of the spheres. After cooling down, HCSs-5-S were obtained.

2.5 Electrochemical measurements

The electrode film of cathode was prepared by mixing the HCSs-S composites, polyvinylidene difluoride (PVDF as a binder) and conductive carbon black with ratios of 80:10:10 to form a homogeneous slurry in *N*-methyl pyrrolidinone (NMP) solvent. The slurry was casted onto aluminum foils and dried at 60 °C for 10 h in a vacuum chamber. The CR2025 coin-type cells were assembled using Li metal as anode and (PP/PE/PP, Celgard) membrane as separator. The electrolyte was composed of a non-aqueous solution obtained by dissolving LiTFSI in a mixture of 1,3-dioxolane and 1,2-dimethoxyethane (1:1, v/v) with 1 M concentration. The electrolyte injected in coin cells is about 60 μL per cell. The galvanostatic charge/discharge tests were carried out in a voltage range of 0.005-3 V on a LAND CT2001A tester. For the rate capability measurements, the current density of charge/discharge gradually increased from 0.1C to 2C and then return to 0.1C. The (CR2025) cells were assembled in a glove box filled with high purity of Ar in which water and oxygen contents were less than 1 ppm.

View Article Online
DOI: 10.1039/C9TA10808D

2.6 Characterization

Fourier transform infrared FT-IR spectroscopy was performed on a NICOLET 6700 spectrometer, equipped with an attenuated total reflection (ATR) setup. Solid-state ^{13}C cross-polarization magic angle spinning (CP-MAS) NMR spectra were obtained on an Agilent DD2-500 MHz at 125.7 MHz, spinning rate of 10 kHz, ^{13}C cross-polarization was performed both using a contact time of 4 s. Field emission scanning electron microscopy (FESEM) images were recorded on a Nova Nano-SEM 450 microscope at an acceleration voltage of 3 kV with a thin platinum layer coated on all samples. Transmission electron microscopy (TEM) images were obtained using Hitachi HT7700 Exalens and FEI Tecnai F30 microscope at 100kV and 300 kV, respectively. N_2 adsorption-desorption isotherms were obtained at -196 °C on a Beishide 3H-2000PM Instrument. Samples were degassed at 300 °C for 6 h prior to analysis. Raman spectra were collected using a DXR Smart Raman (Thermo Fisher) with an excitation laser wavelength of 633 nm. Elemental analysis was obtained on an Elementar UNICUBR (CHN). X-ray photoelectron spectroscopy (XPS) analysis was measured by making use of a Thermo VG ESCALAB 250 with an Al Kα X-ray source operating at 150 W (15 kV). UV/Vis/NIR absorbance and optical turbidity measurements were recorded on a Lambda 750S UV-Vis-NIR spectrophotometer equipped with a a Starna stirred cuvette. The sulfur content of the sample was monitored using a CS-8800 Type Infrared Carbon & Sulphur Analysis Instrument.

3. Results and discussion

The standard preparation of HPSs was shown in Scheme 1. Briefly, a certain amount of *m*-phenylenediamine (*m*-PD), melamine and 3,5-diaminobenzoic acid (DABA) were added to a mixture of acetone and water. In the mixture, *m*-PD and DABA were completely dissolved, while

View Article Online
DOI: 10.1039/C9TA10808D

melamine was slightly soluble in the solvent. So, the concentrations of DABA and *m*-PD are much higher than that of melamine. Schiff base reaction happened between formaldehyde and DABA firstly, then the formed intermediate imine groups of DABA grew linearly with high concentration of *m*-PD rather than melamine by the addition reaction between imine and amino groups (see Fig. S1a for detail).[31, 32] In a very short interval, inner polymer spheres with low degree of polymerization were formed due to the fast precipitation and encapsulation.[26, 31] With the quick formation of inner polymer spheres, the concentration of *m*-PD would be rapidly reduced and its reaction speed was not fast enough for further polymer formation. While the undissolved melamine started to dissolve gradually and reacted with imine groups of DABA to form network which mainly generated the outer shell of the spheres. Polymer spheres have interwoven structure of outer shell with high degree of polymerization due to the gradual encapsulation and continuous supply of reactant[26]. Finally, the solid polymer spheres (SPSs) with polymer from *m*-PD and DABA as core and polymer from melamine and DABA as shell formed. This reaction process is similar to heterogeneous nucleation and growth theory in which reactant with high concentration will burst to form inner core of the spheres, while the reactant with low concentration will react gradually and form shell of the spheres.[33]

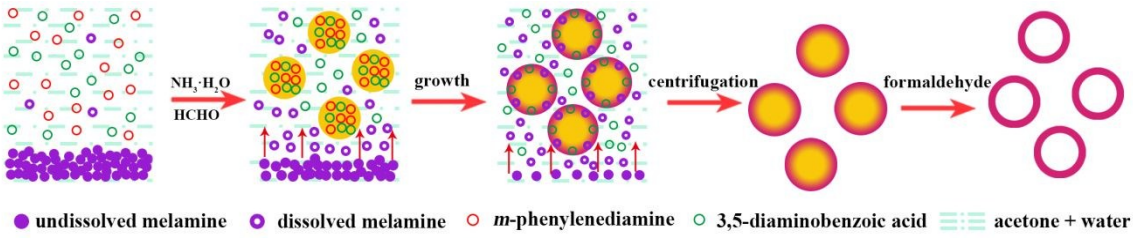

Scheme 1. Illustration of the HPSs synthetic process.

The HPSs were produced by adding the as-synthesized SPSs into formaldehyde solution

View Article Online
DOI: 10.1039/C9TA10808D

(37%~40%), which can dissolve the inner component owing to the reversibility of both Schiff base reaction and addition reaction of imines.[34, 35] Meanwhile, the properties as linear structure and low polymerization degree of the polymer also contribute to this process.[31] The scheme of dissolving procedure is illustrated in Fig. S1b. Basically, addition reaction is reversible and it reached the stage of equilibrium after SPSs formed. High concentration of HCHO led to the sharp decline of amidogen content of inner core breaking the equilibrium of addition reaction. Therefore, the addition product of inner core decomposed readily and provided more amino groups into the solution owing to the linear structure with low stability. Difference between the stability of inner linear structure and outer framework of polymer and different degree of polymerization are the main reasons for producing hollow structure. Because the dissolution of inner linear structure is easier than external framework of polymer.[36] Mass spectrum shows a peak at 155.2 m/z (Fig. S2) corresponding to $[M+Na]^+$ which indicates that large number of imines are formed from the inner polymer decomposition in formaldehyde solution through the reversible Schiff base reaction. In order to maximize the utilization of formaldehyde, we recycled the remaining formaldehyde from solution after extracting SPSs as a reactant to obtain the hollow nanospheres. As shown in Fig. S3, the morphology and hollow structure of the nanospheres are well maintained, indicating the successfully reusing of recovery liquid after formaldehyde solution treatment.

To prove the mechanism we proposed, the solubility of three ingredients were firstly studied. The *m*-PD and DABA are soluble in both acetone and water, while melamine is insoluble in acetone and slightly soluble in water (2.56×10^{-2} mol/L),[37-39] which can also be observed from Fig. S4. The difference of reaction rate between *m*-PD and melamine reacting with DABA in pure water could also be observed through the color change over time (Fig. S5) and the graph of

View Article Online
DOI: 10.1039/C9TA10808D

time-dependent absorption changes (Fig. S6). The solubility control mechanism was further demonstrated by tuning the ratio of acetone and water, as shown in Fig. 1. When pure acetone was employed as the solvent, the SPSs could be obtained, however, no HPSs were left after formaldehyde solution treating. It can be explained that only unstable linear polymer spheres with low degree of polymerization were formed by the chemical combination of DABA, *m*-PD and formaldehyde, but no stable shell due to the insolubility of melamine in acetone. When the volume of water was increased to 2.5 mL, there were also no HPSs but some fragments left after adding the SPSs to formaldehyde solution, which can be attributed to the fragile thin shell constituted by insufficient soluble melamine (Fig. S7a). Continuously increasing the volume of water to 5 mL, uniform HPSs with 60 nm thick shell were obtained which are presented in Fig. S7b. Furthermore, with the ratio of water/acetone growing, there were only solid spheres produced after formaldehyde solution treatment (Fig. S7c and d), which can be explained that the partial dissolved melamine was enough to take part in the formation of polymer spheres in the nucleation stage, making the inner structure stable and insoluble in formaldehyde solution. The size of SPSs become smaller in 50 mL water than in 10 mL water. This could be explained that the amount of nuclei increases with raising concentration of melamine and less monomers can be received by each nucleus.

View Article Online
DOI: 10.1039/C9TA10808D

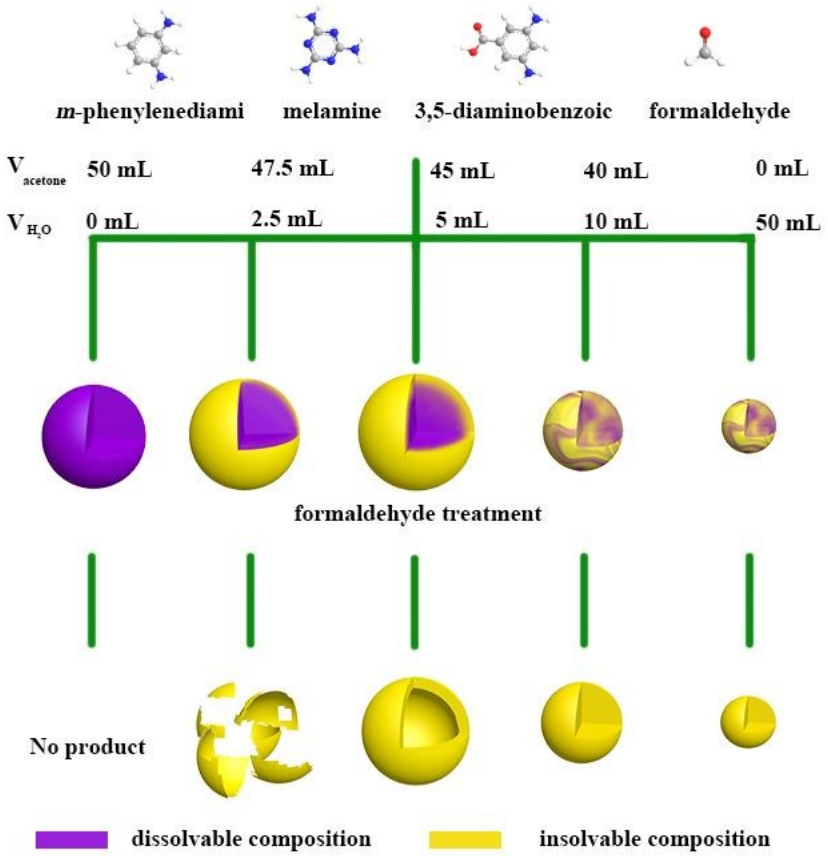

Fig. 1 Schematic illustration of the different shape and structure of spheres via tuning the ratio of acetone and water.

The constitution of HPSs was deeply investigated to shed light on the formation mechanism. ^{13}C solid-state NMR analysis was performed to ascertain the structure of HPSs. The ^{13}C cross-polarization magic angle spinning (CP-MAS) NMR spectrum of HPSs (Fig. 2) shows seven resonances at 172, 167, 144, 132, 102, 101, and 70 ppm, respectively. The weak peak of 172 ppm could be ascribed to carboxyl-C. The signal at 167 ppm can be attributed to the carbon atoms on triazine ring of the melamine, whereas the signals at 144, 132, 102, 101 ppm originates from the CH aromatic carbons of the benzene ring of DABA. The resonance at 70 ppm could be assigned to the secondary carbon atoms formed upon addition of the primary amine groups of melamine to the

View Article Online
DOI: 10.1039/C9TA10808D

newly formed imine double bond. [31, 32] Those reflected the fact that the DABA and melamine were successfully incorporated into HPSs, which is similar to previously reported.[32] Meanwhile, SPSs were also performed ^{13}C solid-state NMR analysis. The peak positions of SPSs were the same with HPSs, while the relative strength of the peaks changed obviously. The relative strength of peak at 167 ppm decreased dramatically due to the presence of inner part of SPSs, which lead to the proportion decrease of carbon atoms on triazine ring (Fig. S8a). In the ^{13}C solid-state NMR spectrum of polymer nanoparticles synthesized from reactants except melamine (the inner part of SPSs), the peak of 167 ppm was not observed while positions of the other peaks were similar with HPSs (Fig. S8b). From the above discussion, it can be concluded that structures of the internal and external part of SPSs were different and the composition of HPSs were also different from SPSs.

The structure of the HPSs was further confirmed by Fourier transform infrared (FTIR) spectroscopy (Fig. 2b). The single absorption peak at approximately 3340 cm^{-1} corresponded to N-H stretching vibration, which demonstrate the present of secondary amine. The stretching vibration mode of C-N (1164 cm^{-1}) and C-N (Ar) (1335 cm^{-1}) and the stretching vibration mode of C=N (1551 cm^{-1}) and out-of-plane bending (811 cm^{-1}) of the triazine ring are present in the spectrum of the polymer shell, indicating the successful incorporation of DABA and melamine into the network.[31, 32] The FTIR spectra of SPSs exhibit a series of adsorption peaks consistent with the HPSs due to the similar peak position of DABA and *m*-PD (Fig. S9). From the discussion above, we further demonstrated that the inner linear structure polymer with low polymerization degree formed from *m*-PD was not stable, while the outer high polymeric netty framework from melamine was stable enough to serve as the shell of HPSs.

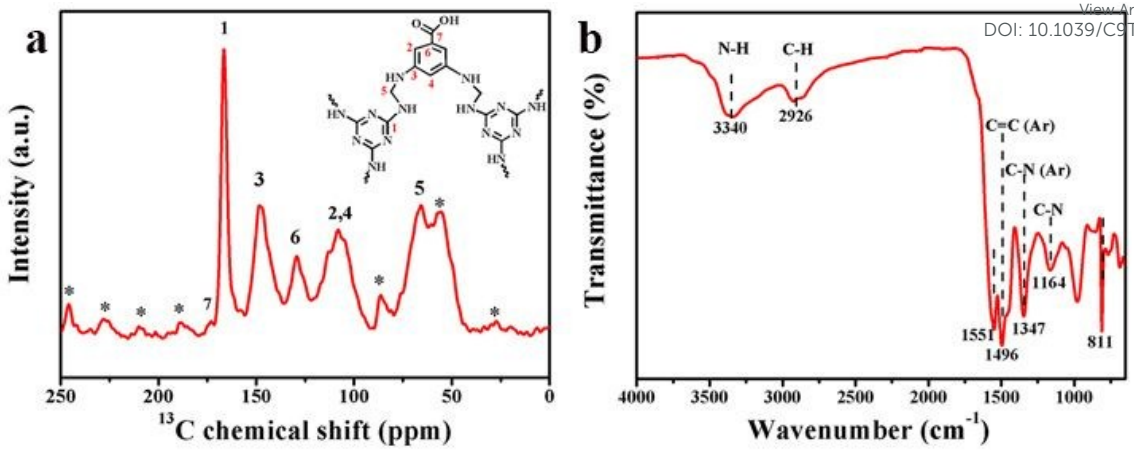

Fig. 2 ^{13}C CP-MAS NMR and FTIR spectra of HPSs. The asterisk denotes spinning side bands.

From the schematic illustration in Fig. 3a, the production of HCSs is simple and efficient. As shown in Fig. 3b-j, the morphology and structure of different spheres were characterized by SEM and TEM. The resulting SPSs and HCSs all exhibit spherical morphology with a smooth surface. The average diameter of SPSs and HCSs was about 600 nm. The TEM (Fig. 3c, d) characterization confirmed that the SPSs possess a solid inside structure. After the formaldehyde treatment, the solid inside of SPSs was dissolved and hollow structured polymer spheres were produced (Fig. 3e). Fig. 3f and g are the TEM image of HPSs, further proving the emergence of hollow structure in the nanospheres with a shell thickness of 62 nm. After calcination at 700 °C, the hollow nanospheres shrunk with the overall structure unchanged, the average particle size decreased from around 600 to around 370 nm and the shell thickness of the obtained HCSs is about 40 nm. After activation with the mass ratio 5:1 of K_2CO_3 and carbon spheres, large amounts of pores can be observed in the HCSs. Most of them are fuzzy wormlike micropores, but there still exists a few of larger pores as marked in red circles in Fig. S10.

View Article Online
DOI: 10.1039/C9TA10808D

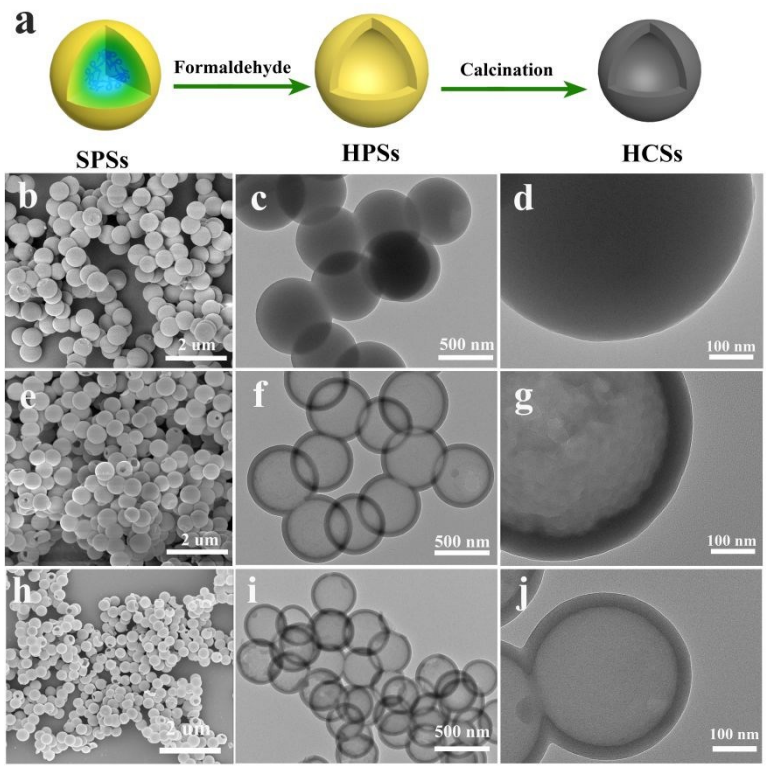

Fig. 3 Schematic illustration of the synthesis route from SPSs to HCSs. SEM and TEM images of SPSs (b-d), HPSs (e-g) and HCSs (h-j).

The key parameters of the hollow structure of the nanospheres can be easily controlled, particularly the size and shell thickness control of nanospheres. By altering the amount of formaldehyde during the synthesis reaction, the size of the spheres can be tuned from 1.5 μm-332.0 nm (Fig. 4). This could be explained that the amount of nuclei increases with raising the formaldehyde dosage in the nucleation stage, which causes less monomers can be received by each nucleus and the size of produced nanospheres are certainly reduced. The thickness of the shell can be altered from 135 nm to 35 nm with changing the duration of formaldehyde solution treatment, which attributed to that more inner polymers can react with formaldehyde. Fig. 4 shows that a prolonged time of dissolving treatment results in a thinner shell together with a larger cavity, which is also an evidence indicating that the outer network is more stable than the inner liner

View Article Online
DOI: 10.1039/C9TA10808D

structure and further demonstrated the reasonability of our mechanistic assumptions. Because the pH has a great influence on Schiff base formation, the amount of ammonia could affect the size, morphology and shell thickness of the spheres as well (Fig. S11). We can also change the size and the shell thickness of the spheres by changing the amount of *m*-PD, melamine as show in Fig. S12 and Fig. S13. The details will be discussed in supporting.

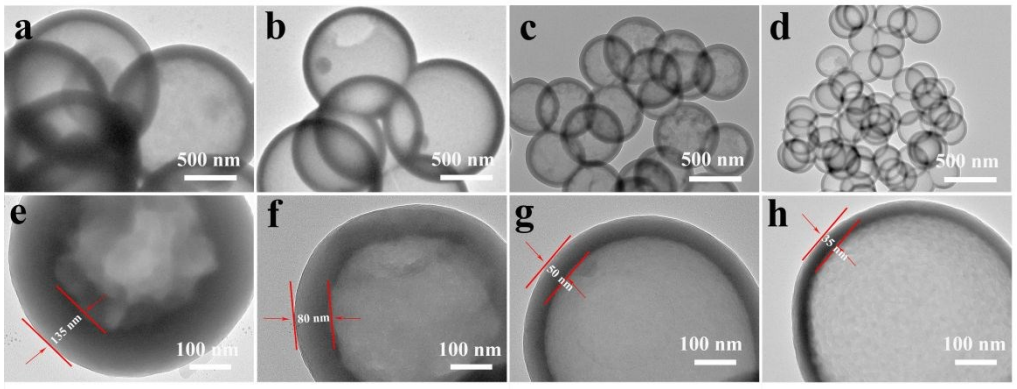

Fig. 4 TEM images of hollow spheres synthesized. (a-d) Size controlled by regulating the amount of formaldehyde in SPSs synthesis process. The mount of formaldehyde in a-d were 0.5 mL, 1 mL, 2 mL, and 4 mL. (e-h) Shell thickness controlled by changing the time of socking in formaldehyde solution. e) 5 min, f) 20 min, g) 4 h, h) 24 h.

N_2 adsorption–desorption experiment was implemented to explore the pore structure. The HCSs-5 exhibit a combined character of type I and type IV isotherm.[40] As shown in Fig. S14, after activation the adsorption isotherm of HCSs show an obvious increase below the relative pressure of $P/P_0 < 0.1$, indicating the existence of abundant micropores. The adsorption hysteresis loop at relative pressures above 0.4 confirms the existence of mesopores in the spheres, which indicates that the hierarchical pore structure exists in the carbon shell. The surface area of the HCSs-5 calculated using the BET equation is as high as 2462.3 m^2g^{-1} and a total pore volume of 1.6 cm^3

View Article Online
DOI: 10.1039/C9TA10808D

g^{-1}. The pore size distribution of the HCSs-5 obtained by using the density functional (DFT) theory shows that the pores were mainly consisted of 1.2-2.0 nm micropores, meanwhile a fraction of mesopores around 2.0-4.0 nm was also existed. The result of the pore size distribution is consisted with the characterization from TEM image (Fig. S10). The existence of micropores and mesopores both play important roles to achieve the excellent cyclic stability and high rate performance of carbon materials.[41, 42] The micropores can effectively confine the small sulfur molecules (S_2-S_4), which can prevent large area contact of sulfur with electrolytes and prohibit side reactions according to the previous reports.[43, 44] Hierarchical porous carbons with tailored pore structure can effective improve the performance of L-S batteries.[45] Thus, the unique hierarchical pores of the as-synthesized HCSs-5 in the shell is beneficial for high stability and enhancing charge transfer during redox cycling.

XPS spectra were carried out to explore the structure information of cathode. From the overall XPS spectrum of the HPCs-S, the C, N, O and S signals were detected (Fig. S15), which confirmed the coexistence of N and O and S in the carbon framework. For the S 2p spectrum of HCSs-S, two peaks at 165.0 eV and 163.8 eV can be observed, which are ascribed to S $2p_{1/2}$ and S $2p_{3/2}$ spin-orbit levels of elemental sulfur.[46] The binding energy of S $2p_{3/2}$ is lower than that of elemental sulfur (164.0 eV), which shows that C–S bond had formed between porous carbon shell sulfur.[39] The weak peak of 167.3 eV can attributed to oxidation of sulfur in the air. The C 1s spectrum can be deconvoluted into four peaks centered at 284.7 eV (C-C/C=C), 285.4 eV (C-O/C-N/C-S), 286.7 eV (C-N-C) and 289.5 eV (sp^2-NH_2). The weak peak of 289.5 eV is assigned to sp^2-hybridized carbon in the aromatic rings attached to NH_2 groups.[2, 47] The C-S bonding is formed during the high heating temperature (400 °C) and doping of nitrogen atoms,

View Article Online
DOI: 10.1039/C9TA10808D

which can improve the performance of electrodes.[2] The N 1s spectrum is further fitted into three peaks at around 398.4, 400.7 and 403.4 eV, which are ascribed to the pyridinic N, pyrrolic N and quaternary N, respectively.[48-51] The abundant N sites in HCSs served as active sites to strongly bind polysulfides (LiPSs), which can greatly enhance the electrochemistry performance of Li-S batteries.

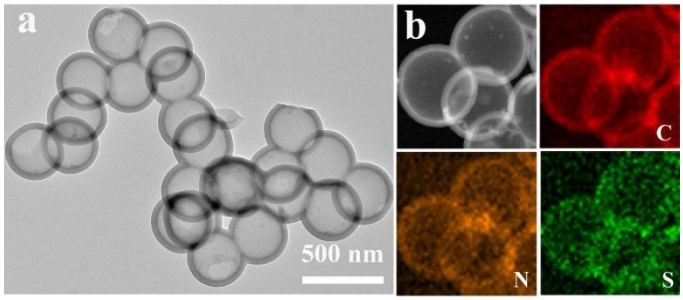

Fig. 5 (a) TEM images of HCSs-5-S and (b) scanning transmission electron microscopy (STEM) image of HCSs-5-S and corresponding elemental mappings of HCSs-5-S.

The structure of HCSs-5-S were further confirmed by TEM, HAADF-STEM and EDS elements mapping (Fig. 5). TEM image of the HCSs-5-S composite after diffusing sulfur into HCSs-5 is shown in Fig. 5a. No obvious sulfur particles could be found outside the HCSs-5-S. To further reveal the element distribution of the HCSs-5-S composite, STEM and the elemental mapping were performed (Fig. 5b). It can be observed from the images that N elements was homogeneously distributed in the carbon shell. From S elemental mapping, sulfur had mostly penetrated through the porous carbon framework into the inside shell and a fraction of sulfur was still accumulated in the carbon wall. Raman spectra were employed to investigate the state of C in HCSs-S and HCSs. As shown in Fig. S16, the D band at 1356 cm^{-1} reflects the sp^3 hybridized

View Article Online
DOI: 10.1039/C9TA10808D

carbon and defects in the structure. While the distinct G band at 1582 cm^{-1} represents the sp^2 hybridized carbon, which are beneficial to fast electron transfer during the electrochemical reaction process.[20] In addition, there is no characteristic signal of sulfur could be found in the Raman spectrum of HCSs-S, implying HCSs act as excellent physical host of sulfur, which is coincident with the high rate performance.[2] Furthermore, large amounts N could provide strong chemical adsorption to trap LiPSs in the cathode, which could reduce the shuttle effect and loss of active sulfur.[52, 53]

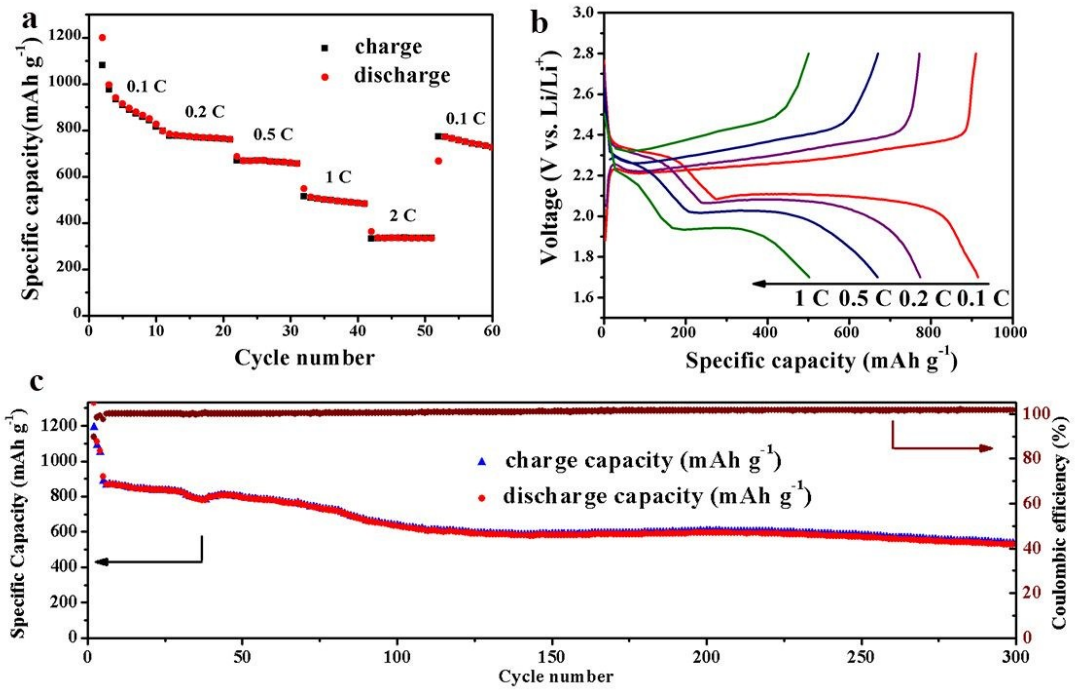

Fig. 6 (a) Rate performance of HCSs-5-S; (b) voltage profiles of HCSs-5-S at different current densities from 0.1 to 1C; (c) coulombic efficiency and prolonged cycle life at 0.5C of the HCSs-5-S electrode.

Our interest in the nitrogen-doped hollow carbon structures as a cathode material for Li–S batteries is inspired by the fact that hollow structure and high nitrogen level should be effective to volumetric expansion and buffer the shuttle effect of LiPSs, which is the major haunted problems

View Article Online
DOI: 10.1039/C9TA10808D

on Li–S batteries. The elemental analysis (Table S1) reveals that the nitrogen content in SPSs, HPSs and HCSs is 21.36%, 26.99% and 12.50%, respectively. The HCS-5-S were mixed with PVDF and carbon black (80:10:10 by weight) to prepare the cathode electrodes. The sulfur ratios in the whole cathode were about 50%, considering the 66% sulfur contents in the composite measured by combustion analysis, using CS-8800 Type Infrared Carbon & Sulphur Analysis Instrument. The electrode films were consisted of a loading of 0.9–1.2 mg cm^2 based on pure sulfur. At first, the HCS-5-S nanospheres were subject to cycling at different charge/discharge current rates ranging from 0.2C to 2C to evaluate the rate property as shown in Fig. 5a. After an initial discharge capacity of 1200 mA h g^{-1} at 0.1C, further increase current at 0.2, 0.5, 1.0 and 2C delivered highly reversible capacities around 755, 642, 481 and 301 mA h g^{-1}, respectively. When the current was switched to 0.1C again, the capacities 755 mA h g^{-1} could be achieved, indicating the good stability of the cathode material. The initial discharge/charge profiles of the HCSs-5–S electrodes at different rates exhibited two obvious discharging platforms, as shown in Fig. 5b, which was the typical multistep reduction of sulfur. After being activated at 0.1C for the first three cycles, the HCSs-5-S electrodes delivered the reversible discharge capacities of 528 mA h g^{-1} even after 300 cycles, corresponding to a capacity retention of 58% (based on the 4th cycle). Meanwhile, the HCSs-5-S delivers a coulombic efficiency were around 100% after 300 cycles (Fig. 5c). The good performance and the novel strategy for fabricating the nitrogen-doped hollow carbon nanospheres endow it a promising candidate for Li-S batteries.

4. Conclusions

In summary, we developed a new synthetic strategy for polymer spheres with tunable inner core and outer shell by controlling the proportion of precursors in acetone/water system, according to

View Article Online
DOI: 10.1039/C9TA10808D

the different solubility of reactants. The hollow structure can be created during the soaking of the as-prepared SPSs in formaldehyde solution, which would dissolve the inner core rather than the outer shell of nanoparticles due to area-specific distribution of polymeric components. The mentioned controlling solubility principles both in the formation and core dissolution process of the spheres, not only provide a new protocol for the hollow structure building, but also demonstrate the formation mechanism of hollow carbon spheres. We can control the size, morphology and shell thickness of spheres by tuning different parameters. The obtained nitrogen-doped HCSs with a hierarchical pore shell can serve as a novel cathode material for Li–S batteries to achieve high-stability and high-capacity performance with a capacity of 528 mA h g^{-1} after 300 cycles at 0.5 C. We hope the proposed effective and versatile strategy for the fabrication of nitrogen-doped hollow carbon spheres can be adapted to other applications such as catalysis, fuel cell and supercapacitor.

Acknowledgments

This work is supported by the Joint Funds of the National Natural Science Foundation of China (U1608223), National Natural Science Foundation of China (21576044, 21536002), the Science Fund for Creative Research Groups of the National Natural Science Foundation of China (21421005), Key Laboratories Basic Research Program of Education Department of Liaoning Province (LZ2015020), Dalian University of Technology Innovation Team (DUT2016TB12) and State Key Laboratory of Fine Chemicals (KF1516).

References

1. G. He, S. Evers, X. Liang, M. Cuisinier, A. Garsuch and L. F. Nazar, *Acs Nano*, 2013, **7**, 10920-10930.

2. Y. Peng, Y. Zhang, J. Huang, Y. Wang, H. Li, B. J. Hwang and J. Zhao, *Carbon*, 2017, **124**, 23-33.

3. X. Gao, Q. Sun, X. Yang, J. Liang, A. Koo, W. Li, J. Liang, J. Wang, R. Li, F. B. Holness, A. D. Price, S. Yang, T. Sham and X. Sun, *Nano energy*, 2019, **56**, 595-603.

4. J. Han, G. Xu, B. Ding, J. Pan, H. Dou and D. R. MacFarlane, *J. Mater. Chem. A,* 2014, **2**, 5352-5357.

5. M. Liu, Y. Yu, B. Liu, L. Liu, H. Lv and A. Chen, *J. Alloy Compd.*, 2018, **768**, 42-48.

6. Y. Wei, X. Zhang, Z. Zhao, H. Chen, K. Matras-Postolek, B. Wang and P. Yang, *Electrochim. Acta*, 2019, **297**, 553-563.

7. J. Chi, W. Gao, L. Zhang, B. Dong, K. Yan, J. Lin, B. Liu, Y. Chai and C. Liu, *ACS Sustainable Chem. Eng.*, 2018, **6**, 7676-7686.

8. M. Y. Song, D. Yang, K. P. Singh, J. Yuan and J. Yu, *Appl. Catal., B*, 2016, **191**, 202-208.

9. X. Lin, Q. Sun, K. Doyle Davis, R. Li and X. Sun, *Carbon Energy*, 2019,1-24.

10. Y. Sun, C. Cao, C. Liu, J. Liu, Y. Zhu, X. Wang and W. Song, *Carbon*, 2017, **125**, 139-145.

11. H. Li, J. Zhao, R. Shi, P. Hao, S. Liu, Z. Li and J. Ren, *Appl. Surf. Sci.*, 2018, **436**, 803-813.

12. J. Chen, K. Liu, M. Jiang, J. Han, M. Liu, C. Wang and C. Li, *Colloids Surf., A*, 2019, **568**, 461-469.

13. J. Qi, Y. Li, G. Wei, J. Li, X. Sun, J. Shen, W. Han and L. Wang, *Sep. Purif. Technol.*, 2017, **188**, 112-118.

14. X. Wu, Y. Si, Y. Zou, Y. Mao, Q. Li, S. Zhou, M. Chen and L. Wu, *ACS Appl. Mater. Interfaces*, 2018, **10**, 31664-31673.

15. W. Zhou, C. Wang, Q. Zhang, H. D. Abruña, Y. He, J. Wang, S. X. Mao and X. Xiao,

View Article Online
DOI: 10.1039/C9TA10808D

Adv. Energy Mater., 2015, **5**, 1401752.

16. T. Yang, Y. Zhong, J. Liang, M. M. Rahman, W. Lei, Y. Chen, M. J. Monteiro, Z. Shao and J. Liu, *Part. Part. Syst. Charact.*, 2017, **34**, 1600281.

17. C. Ye, L. Zhang, C. Guo, D. Li, A. Vasileff, H. Wang and S. Qiao, *Adv. Funct. Mater.*, 2017, **27**, 1702524.

18. M. Chen, Q. Lu, S. Jiang, C. Huang, X. Wang, B. Wu, K. Xiang and Y. Wu, *Chem. Eng. J.*, 2018, **335**, 831-842.

19. Z. Li, J. Zhang, B. Guan, D. Wang, L. Liu and X. W. Lou, *Nat. Commun.*, 2016, **7**.

20. M. Fang, Z. Chen, Y. Liu, J. Quan, C. Yang, L. Zhu, Q. Xu and Q. Xu, *J. Mater. Chem. A,* 2018, **6**, 1630-1638.

21. C. Zhang, H. B. Wu, C. Yuan, Z. Guo and X. W. Lou, *Angew. Chem., Int. Ed.*, 2012, **51**, 9592-9595.

22. J. Lin, W. Zhao, M. Qian, K. Liu, J. Xu and F. Huang, *Chem. Commun.*, 2018, **54**, 4565-4568.

23. G. Wang, Q. Sun, R. Zhang, W. Li, X. Zhang and A. Lu, *Chem. Mater.*, 2011, **23**, 4537-4542.

24. F. Xu, Z. Tang, S. Huang, L. Chen, Y. Liang, W. Mai, H. Zhong, R. Fu and D. Wu, *Nat. Commun.*, 2015, **6**.

25. L. Chai, W. Yu, H. Wang and L. Zhang, *Micro Nano Lett.*, 2012, **7**, 1264-1266.

26. D. Bin, Z. Chi, Y. Li, K. Zhang, X. Yang, Y. Sun, J. Piao, A. Cao and L. Wan, *J. Am. Chem. Soc.*, 2017, **139**, 13492-13498.

27. B. Liu and H. C. Zeng, *Small*, 2005, **1**, 566-571.

28. F. Ma, H. Zhao, L. Sun, Q. Li, L. Huo, T. Xia, S. Gao, G. Pang, Z. Shi and S. Feng, *J. Mater. Chem.*, 2012, **22**, 13464.

View Article Online
DOI: 10.1039/C9TA10808D

29. H. C. Zeng, *Curr. Nanosci.,* 2007, **3**, 177-181.

30. S. Luo, J. Li, X. Zhang, Q. Lin and C. Fang, *J. Anal. Appl. Pyrolysis*, 2018, **135**, 10-14.

31. Y. Liu, M. Liu, W. Ye, H. Huang, H. Lin, X. Ren, R. Lu and S. Zhang, *Mater. Res. Express*, 2019, **6**, 85097.30.

32. M. Liu, Y. Liu, Z. Gao, C. Wang, W. Ye, R. Lu and S. Zhang, *New J. Chem.*, 2018, **42**, 15962-15967.

33. J. Song, F. Tronc and M. A. Winnik, *J. Am. Chem. Soc.*, 2004, **126**, 6562-6563.

34. L. R. W, *Chem. Rev.*, 1962, **63**, 489-510.

35. Y. Xin and J. Yuan, *Polym. Chem.*, 2012, **3**, 345-355.

36. K. Jin and J. M. Torkelson, *Macromolecules*, 2016, **49**, 5092-5103.

37. P. Lian, H. Zhao, J. Wang, L. Chen, Y. Xiang and Q. Ren, *Chin. J. Chem. Eng*., 2019, **27**, 1149-1158.

38. R. P. Chapman, P. R. Averell and R. R. Harris, *Ind. Eng. Chem.*, 1943, **35**, 137-138.

39. C. Bretti, C. De Stefano, G. Lando and S. Sammartano, *Fluid Phase Equilib*., 2013, **355**, 104-113.

40. T. Wang, Y. Sun, L. Zhang, K. Li, Y. Yi, S. Song, M. Li, Z. A. Qiao and S. Dai, *Adv. Mater.*, 2019, **31**, 1807876.

41. G. He, S. Evers, X. Liang, M. Cuisinier, A. Garsuch and L. F. Nazar, *Acs Nano*, 2013, **7**, 10920-10930.

42. H. Xu, Y. Deng, Z. Zhao, H. Xu, X. Qin and G. Chen, *Chem. Commun.,* 2014, **50**, 10468-10470.

43. S. Xin, L. Gu, N. Zhao, Y. Yin, L. Zhou, Y. Guo and L. Wan, *J. Am. Chem. Soc.,* 2012, **134**, 18510-18513.

44. S. Niu, G. Zhou, W. Lv, H. Shi, C. Luo, Y. He, B. Li, Q. Yang and F. Kang, *Carbon*, 2016, **109**,

View Article Online
DOI: 10.1039/C9TA10808D

1-6.

45. P. Strubel, S. Thieme, T. Biemelt, A. Helmer, M. Oschatz, J. Brückner, H. Althues and S. Kaskel, *Adv. Funct. Mater.*, 2015, **25**, 287-297.

46. D. Yang, W. Ni, J. Cheng, Z. Wang, T. Wang, Q. Guan, Y. Zhang, H. Wu, X. Li and B. Wang, *Appl. Surf. Sci.*, 2017, **413**, 209-218.

47. Z. Meng, S. Li, H. Ying, X. Xu, X. Zhu and W. Han, *Adv. Mater. Interfaces*, 2017, **4**, 1601195.

48. D. Guo, H. Wei, X. Chen, M. Liu, F. Ding, Z. Yang, Y. Yang, S. Wang, K. Yang and S. Huang, *J. Mater. Chem. A*, 2017, **5**, 18193-18206.

49. G. Zhou, Y. Zhao and A. Manthiram, *Adv. Energy Mater.*, 2015, **5**, 1402263.

50. Y. Zhang, K. Sun, Z. Liang, Y. Wang and L. Ling, *Appl. Surf. Sci.*, 2018, **427**, 823-829.

51. J. Song, M. L. Gordin, T. Xu, S. Chen, Z. Yu, H. Sohn, J. Lu, Y. Ren, Y. Duan and D. Wang, *Angew. Chem., Int. Ed.*, 2015, **54**, 4325-4329.

52. Z. Xiao, D. Kong, Q. Song, S. Zhou, Y. Zhang, A. Badshah, J. Liang and L. Zhi, *Nano Energy*, 2018, **46**, 365-371.

53. J. Song, T. Xu, M. L. Gordin, P. Zhu, D. Lv, Y. Jiang, Y. Chen, Y. Duan and D. Wang, *Adv. Funct. Mater.*, 2014, **24**, 1243-1250.

View Article Online
DOI: 10.1039/C9TA10808D

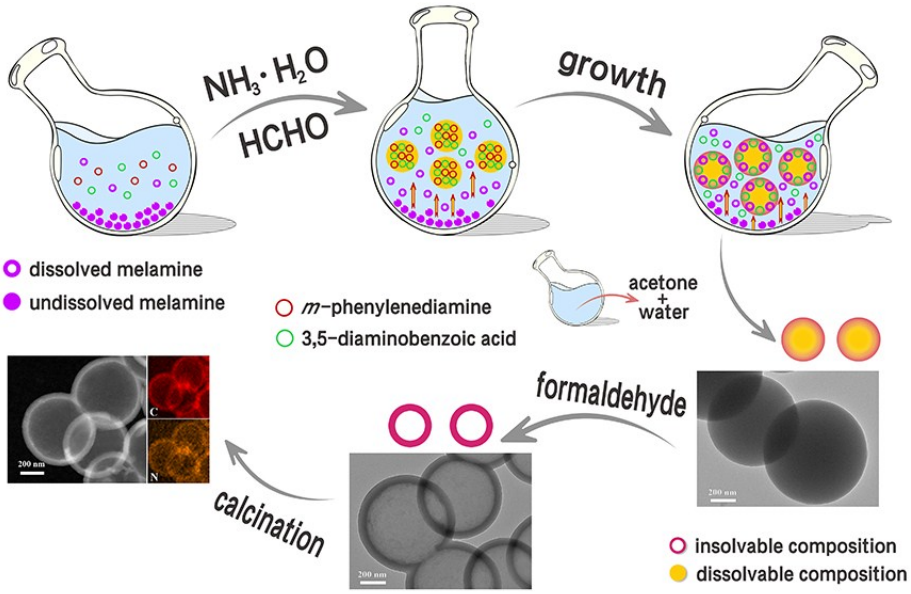

A new protocol to synthesize nitrogen-doped hollow carbon nanospheres by controlled compositional distribution of polymeric component, followed by post-treating of formaldehyde solution.